Available online at www.sciencedirect.com
ScienceDirect
International Journal of Mass Spectrometry 272 (2008) 91–97
International Journal of Mass Spectrometry
www.elsevier.com/locate/ijms

Short communication

Sputtering of nanoparticles: Molecular dynamics study of Au impact on 20 nm sized Au nanoparticles

Steffen Zimmermann, Herbert M. Urbassek *

Fachbereich Physik, Universität Kaiserslautern, Erwin-Schrödinger-Straße, D-67663 Kaiserslautern, Germany

Received 23 November 2006; received in revised form 8 January 2008; accepted 9 January 2008
Available online 31 January 2008

Abstract

Using molecular dynamics simulation we study the sputtering of Au nanoparticles (diameter 20 nm) by 16 and 64 keV Au projectiles. The sputter yield is more than a factor of two larger than for sputtering of a planar target. This feature is connected to a reduced projectile range in the nanoparticle, which leads to shallow energy deposition and pronounced spike sputtering. The sputter yield shows only little dependence on the impact parameter of the nanoparticle. Even at peripheral impacts at 9 nm from the nanoparticle centre, the sputter yield has decreased by only 20% compared to central impacts. Sputter emission accelerates the nanoparticle in the opposite direction to velocities of several m/s.

PACS: 79.20.Rf; 79.20.Ap; 61.80.Lj

Keywords: Sputtering; Nanoparticle; Molecular dynamics

1. Introduction

Ion bombardment and sputtering of nanoparticles form an interesting subject, both from a fundamental and an applied point of view. As to the latter aspect, the compositional analysis of dust and aerosol particles requires an understanding of sputtering, if techniques like the secondary ion mass spectrometry (SIMS) or secondary neutral mass spectrometry (SNMS) are employed [1]; as an example, soot nanoparticles have been investigated by these techniques [2]. In dusty plasmas, dust particles are subject to a flux of energetic ions [3]. In astrophysics, dust grains are irradiated by stellar winds and cosmic rays; the resulting chemical and physical modification of interstellar and interplanetary dust grains is actively being investigated [4–6].

Sputtering of nanoparticles can deviate in two respects from the well-known [7] sputtering of planar surfaces: (i) the nanoparticle provides a *finite system*; the energy deposited by the projectile cannot be conducted away as in a semi-infinite solid. This may lead to abundant sputtering and even complete particle disintegration if the energy density in the nanoparticle surpasses its total binding energy. This case was investigated in a previous paper [8], where a 8 nm Au nanoparticle was irradiated by 100 keV Au atoms, giving rise to an average energy density of 6.3 eV/atom in the nanoparticle. Accordingly violent nanoparticle disintegration events could be observed. (ii) The *surface curvature* of the nanoparticle becomes important as soon as the projectile range is not vanishingly small compared to the nanoparticle radius. Here, more abundant sputtering can be expected than for a planar target, since the collision-cascade or spike volume, where the projectile energy has been deposited is locally closer to the surface and thus has a higher efficacy of inducing surface emission. It is this case which we want to investigate in the present paper.

While atom bombardment of (free) nanoparticles may be more difficult to perform than the sputtering of bulk targets, the bombardment of nanoparticles deposited on surfaces has indeed been investigated experimentally recently [9–11].

The molecular–dynamics simulation of ion interaction with free size-selected clusters is actually simpler to perform than that of bulk targets. The simulation of a free cluster requires no boundary conditions, such as they are needed in their bulk counterpart to take care of the energy dissipation to the surroundings. Thus, several studies of the interaction of swift ions in the electronic-stopping regime with dust particles have been published [4,6]. Also, the disintegration of clusters by

* Corresponding author.
E-mail address: urbassek@rhrk.uni-kl.de (H.M. Urbassek).
URL: http://www.physik.uni-kl.de/urbassek/ (H.M. Urbassek).

1387-3806/$ – see front matter © 2008 Elsevier B.V. All rights reserved.
doi:10.1016/j.ijms.2008.01.004

energetic ion bombardment in the nuclear-stopping regime has been investigated [8]. This study has been extended to the atom interaction with nanoparticles deposited on a surface [12].

Here, we present molecular–dynamics simulations of the sputtering of a Au nanoparticle of 20 nm diameter by 16 and 64 keV Au atoms. In the first case, the ion energy is deposited close to the surface; thus we are in the regime, where the projectile penetration depth is smaller than the nanoparticle radius. For this impact energy, we also study peripheral impacts. At 64 keV, the projectile energy is deposited in the centre of the nanoparticle. Even though complete disintegration events are not observed, the nanoparticle shape is usually deformed drastically.

2. Method

Our spherical Au nanoparticle with radius $R = 10$ nm contains $N = 246{,}697$ atoms. The sphere was constructed by cutting it out of a Au crystal; it hence originally possesses an fcc crystal structure. Before the start of the simulation, the nanoparticle is allowed to relax to relieve all internal stresses. For central impact, the projectile impinges on a local (1 1 1) facet, i.e. along a [1 1 1] direction. For each impact parameter, we simulate a number of 9 impact events by varying the impact points in a region of size 2.2 Å ×3.2 Å, corresponding to the irreducible unit cell of the (1 1 1) surface. For the purpose of comparison, we also performed a sputter simulation for a Au crystallite with a planar (1 1 1) surface. This crystallite contains 1.495×10^6 atoms and employs damping boundary conditions at all but the top surface; further details of this simulation are given in Refs. [13,14]. We choose this particular surface orientation, since its sputtering by atom and cluster impact has been studied (for the planar target) particularly intensely in the past [13–20].

We employ a standard molecular dynamics code [15,21]. The simulation is run until 100 ps after atom impact. The choice of an appropriate interatomic interaction potential is of prime importance for modelling sputtering phenomena under spike conditions [22–24]. Since, obviously, melting may play an important role in spike sputtering, we chose a Au–Au interaction potential, which correctly reproduces the melting temperature of Au [13,14]. Towards high energies, the potential has been splined to the ZBL potential [25]. Electronic stopping has been disregarded in this study. Note that the energy sharing between the electronic and the atomic system is not as important for metallic nanoparticle sputtering as for the sputtering of a bulk metal target, since the nanoparticle volume is comparatively small and the impact energy cannot be transported far away from the spike volume. Furthermore, in the case of Au, electron–phonon coupling is expected to be particularly small [26,27].

3. Results

3.1. 16 keV Impact

Fig. 1 displays perspective views, and Fig. 2 the corresponding cross-sectional views of 16 keV impacts on a planar surface and on a nanoparticle with a central and a peripheral impact

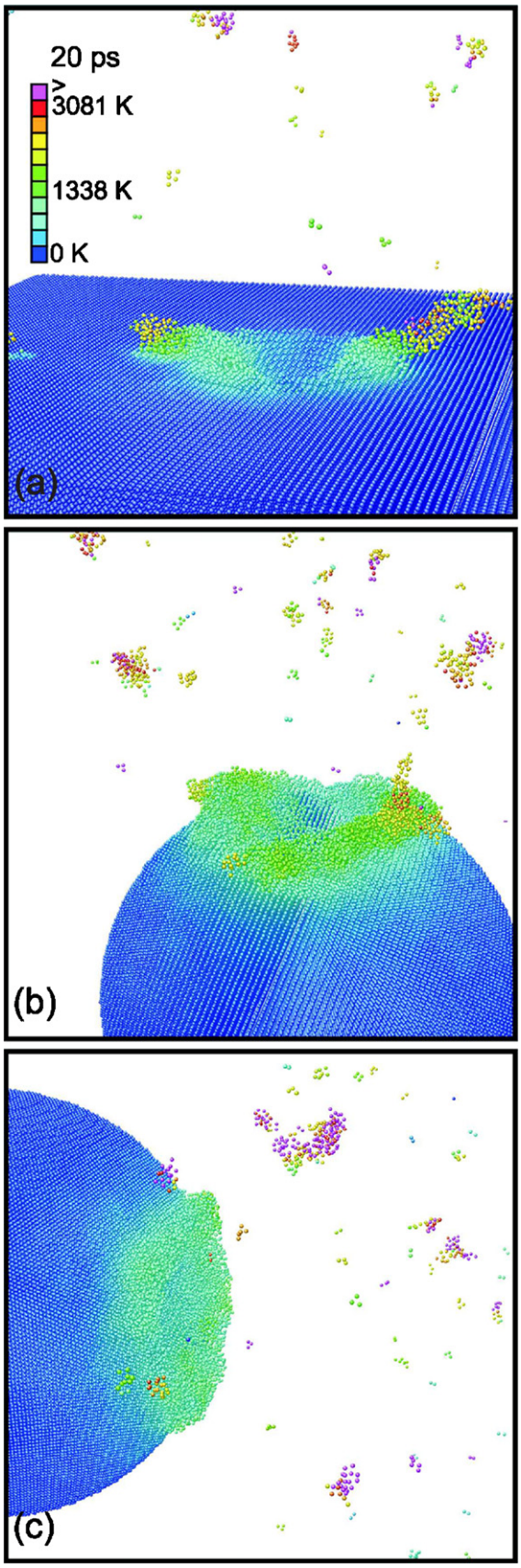

Fig. 1. Perspective view of 16 keV Au impact on a plane surface (a) and on a nanoparticle with impact parameter $b = 0$ (b) and $b = 9$ nm (c) at a time $t = 20$ ps after impact. In each case, representative events have been selected with approximately average sputter yields. Colour denotes the local temperature.

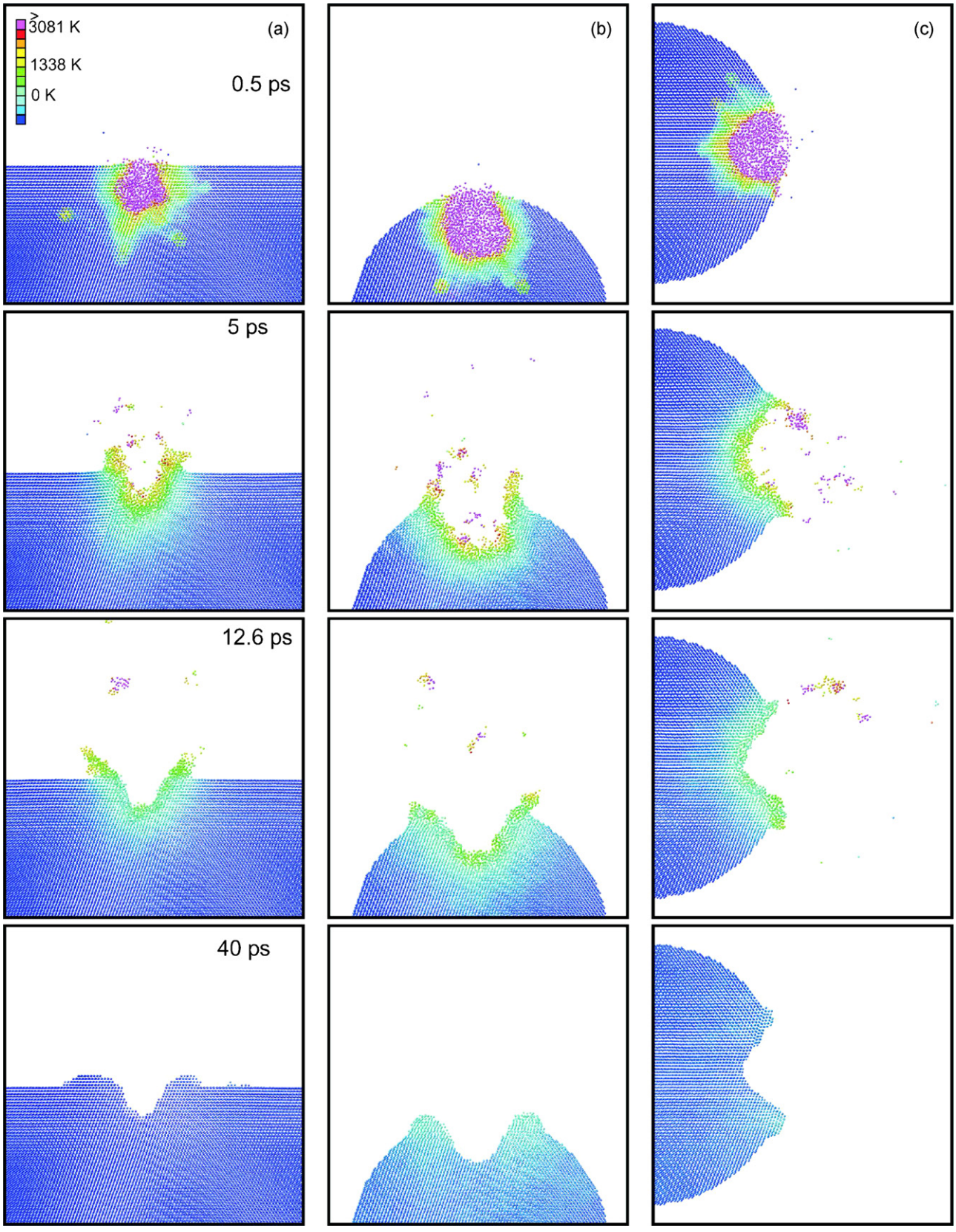

Fig. 2. Cross-sectional view of the time evolution of the events of Fig. 1. The time instants, indicated in subfigure (a), have been chosen identical in the three cases. Colour denotes the local temperature. As in Fig. 1, the projectile impacts vertically downward in all three subfigures.

parameter. In each case representative events, i.e., such with approximately average sputter yields, have been selected. Note that a 16 keV projectile heats the nanoparticle only moderately. If the total impact energy E_0 is distributed among all N atoms, the resulting temperature is only $T = E_0/3Nk = 251$ K, where k is Boltzmann's constant. The shallow energy deposition generates a spike, in which the energy density is so high that the solid material gasifies and explodes into the vacuum. A crater is left behind. The crater walls and the resulting crater rims are liquid and highly mobile; they may give rise to delayed emission of large sputtered clusters. This process has been described previously in detail for a planar target [16].

By comparing the sputtering for a planar target and a nanoparticle, we observe that the crater in the nanoparticle is deeper and, in particular, opens up wider in the nanoparticle. As Fig. 2 shows, the reason for the different crater shapes is connected to the reaction of the surrounding material on the energized spike volume. Whereas the opening of the crater takes only a few pecoseconds, its final form is only reached after >10 ps. While at early times, it is primarily elastic stresses which deform the surrounding medium, later also melt flow on the crater walls and rims influences the form of the crater. Thus for the nanoparticle with its curved surface, even for identical initial energy deposition in the material, the resulting crater will look different than for a planar target. We note that for deeper energy deposition, as reached by 64 keV projectile impact, the forces exerted on the nanoparticle during crater formation are even stronger, cf. Fig. 6.

Peripheral impact leads to a spike scenario, which is quite analogous to that for central impact. The exact location of the impact point of the projectile on the nanoparticle appears to play only a minor role in the spike evolution. The symmetry of the crater is determined more by the local surface normal than by the impact direction.

Fig. 3 displays the average time evolution of sputtering during the first 40 ps after impact; by this time, the sputter yield has reached its final value, cf. Table 1. We see that sputtering occurs in the first 30 ps after projectile impact; the time scale does not sensitively depend on the choice of the surface (planar or spherical) nor on the impact parameter.

Fig. 4 gives a synopsis of the dependence of the sputter yield on the impact parameter b, cf. Table 1. Note that due to the nanoparticle curvature, a non-vanishing impact parameter corresponds to an oblique impact angle ϑ_0, via $\sin\vartheta_0 = b/R$, on the nanoparticle surface. The dependence of the sputter yield on the impact parameter is very mild. For $b \leq 6$ nm ($\vartheta_0 < 37°$), no dependence can be observed within statistical accuracy. Only for the peripheral impact, $b = 9$ nm (corresponding to $\vartheta_0 = 64°$), a slight decrease of the sputter yield by around 20% can be observed.

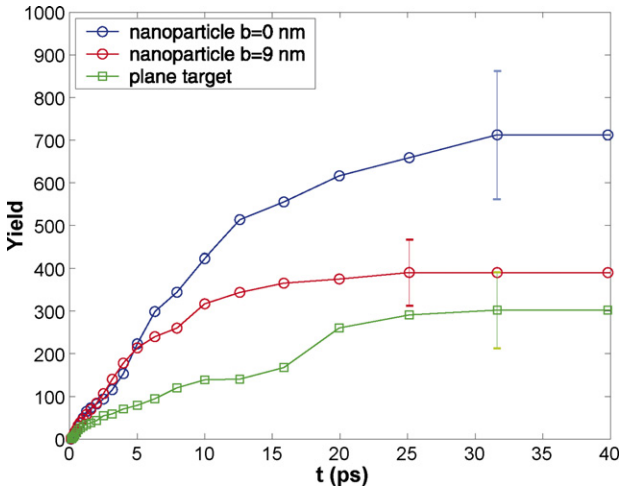

Fig. 3. Time evolution of the average sputter yield of the nanoparticle (impact parameter $b = 0$ and $b = 9$ nm) and of the planar surface. Error bars denote mean error, $\epsilon = \sigma/3$.

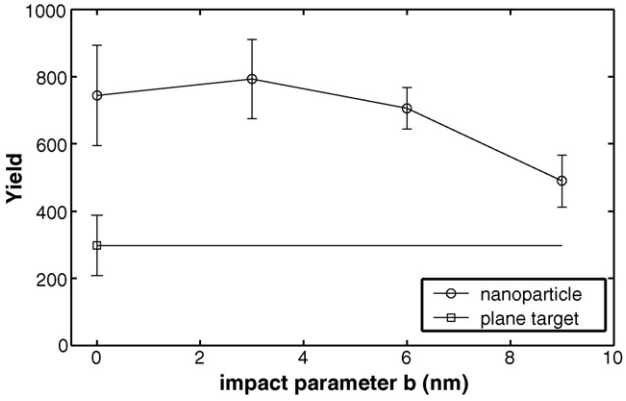

Fig. 4. Dependence of the average sputter yield of the nanoparticle on the impact parameter b. The sputter yield of a planar surface has been included for comparison.

Table 1
Simulation results for the sputtering of a 20 nm Au nanoparticle as a function of impact parameter b and of a planar Au (1 1 1) surface for two different impact energies

	16 keV impact					64 keV impact	
	$b = 0$	$b = 3$ nm	$b = 6$ nm	$b = 9$ nm	Planar target	$b = 0$	Planar target
Y	744	793	706	489	298	2955	616
ϵ	149	118	62	77	90	1392	285
σ	450	355	186	230	271	4176	854
V_{trans} (m/s)	2.1	2.5	2.6	3.5	–	6.5	–
E_{trans} (eV)	1.5	1.8	1.8	3.4	–	19.0	–

Data taken at the end of the simulation, at $t = 100$ ps after projectile impact. Y: average sputter yield. ϵ: statistical error of the average yield. σ: standard deviation of the sputter-yield distribution. V_{trans}: average translational velocity of the nanoparticle at 100 ps after impact. E_{trans}: its translational energy.

For comparison, we also included the sputter yield for a planar surface in the plot. It is smaller by a factor of 2.5 than the sputter yield of the nanoparticle (central impact). This difference may be related to the fact that the projectile range in the nanoparticle is considerably smaller than in the bulk crystal: 1.0 ± 0.4 nm compared to 2.6 ± 0.9 nm. We assume that this range reduction is due to the surface relaxation of the nanoparticle, which reduces the crystalline order at the surface and thus makes channelling of the projectile in the nanoparticle improbable.

3.2. Discussion

There are no experimental or other simulational data on the sputtering of Au nanoparticles with which to compare our results. However, the sputtering of the Au (1 1 1) surface has been investigated quite intensely in the recent past, and we can compare our data for the planar surface with these studies.

Our sputter yield of the plane Au (111) surface amounts to $Y = 298 \pm 90$ (Table 1) [13,28]. This is a rather high value, if compared, e.g., with experimental data [29] for 16 keV Xe → Au (1 1 1) sputtering, which are around $Y = 30$. However, also other simulational studies find high sputtering yields under spike conditions; thus, Salonen et al. [17] calculated $Y \cong 300$ for 25 keV Au impact on Au (1 1 1), in good agreement with our result. The origin of the discrepancy between these large yields and experiment is presently under discussion [18,19,23,24]. Among others, the following reasons are being debated: (i) the attractive part of the interatomic potential is only poorly known in the range of high temperatures and pressures and low particle densities relevant for the spike region. Small changes of the potential may lead to large changes in the melting point and the surface tension of Au; both quantities are known to have a major influence on spike sputtering. In fact, simulation studies using the same high-energy potential, but different low-energy binding potentials give rise to quite different (lower) sputter yields [15,20]. For example, Ref. [15] obtained $Y = 65 \pm 16$; here a potential was used which overestimates the melting point of Au. As a consequence, the contribution of spike sputtering was found to be strongly suppressed; sputtering terminates earlier (after around 10 ps, rather than the 30 ps shown in Fig. 3). (ii) Energy loss of Au atoms to electrons by electron–phonon coupling is usually disregarded in the simulations; since the magnitude of this effect is not fully clear, it can, however, have a major effect on spike quenching in bulk materials [30,31]. (iii) Further effects, such as the polycrystallinity of the sample, atomic surface roughness, fragmentation and back-deposition of emitted clusters, may affect the yields of bulk targets.

In view of the uncertainties described above, we conclude that the analysis of the data obtained in the present study should focus on a discussion of the qualitative, rather than quantitative features.

3.3. Translational velocity of the irradiated nanoparticle

Fig. 5 displays the translational velocity V_{trans} of the nanoparticle, i.e., the velocity of the centre of mass of all atoms which still belong to the nanoparticle, at the end of the simulation. Each arrow represents one simulation event. The pertinent data are also collected in Table 1. It is seen that the nanoparticle obtains a speed in the range of 2–3.5 m/s. The pertinent translational ener-

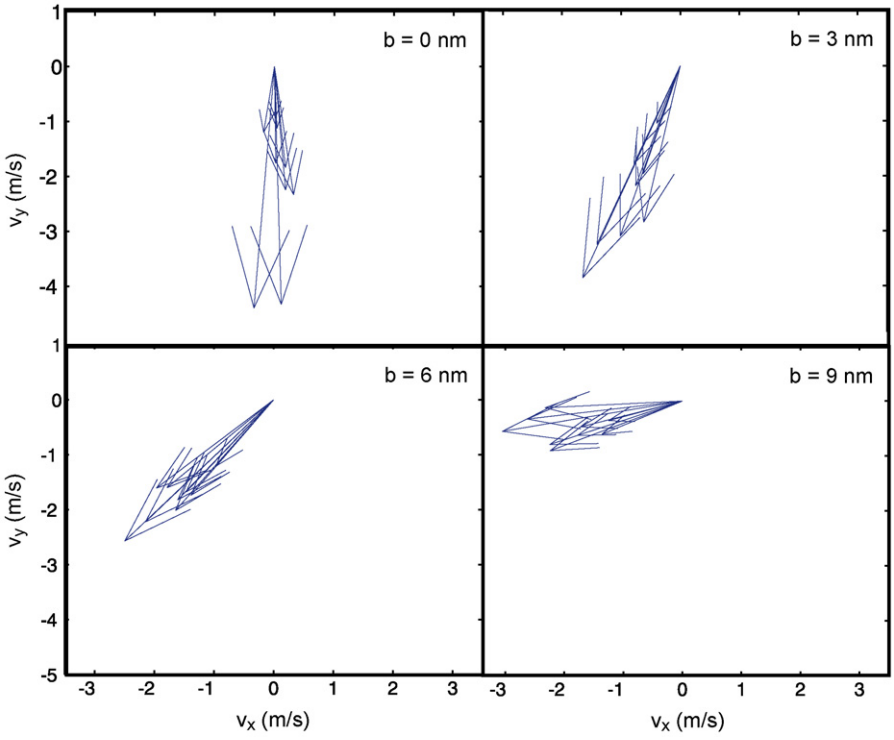

Fig. 5. Translational velocity of the nanoparticle at time $t = 100$ ps after 16 keV Au atom impact, projected into a plane containing the impact velocity (y-axis). Each arrow presents the result of one particular impact event.

gies of the nanoparticle after impact only reach $E_{trans} \cong 1$–10 eV (Table 1); this demonstrates that the projectile–nanoparticle collision is strongly inelastic, in the sense that the projectile energy is dissipated in the nanoparticle and used to heat and sputter it; only a tiny fraction goes into translational motion of the nanoparticle centre of mass.

Let us discuss the collision from the point of view of the *momentum* balance. For a central, totally inelastic collision, in which the projectile sticks to the target – and ignoring sputtering for the moment – the projectile impact accelerates the nanoparticle only to a velocity

$$V_0 = \frac{v_0}{N+1} \cong 0.5\,\mathrm{m/s}. \quad (1)$$

where $N = 246{,}697$ is the number of atoms in the nanoparticle, and $v_0 = 125$ km/s is the projectile velocity. The nanoparticle would drift with this velocity V_0 along the projectile impact direction, $\vartheta = 0°$. As Fig. 5 demonstrates, actual translational velocities of the nanoparticle are definitely larger and are - except for central impact - not directed along the impact direction. This demonstrates that the recoil of the sputtered particles is essential for describing the momentum balance, and hence the nanoparticle translational velocity.

We note that recent simulations [32] of impacts of Au_{400} clusters at 40 keV impact energy on smaller Au nanoparticles (radius of 3 nm, atom number around 6000) show a different behaviour; there nanoparticle accelerations up to $E_{trans} > 100$ eV have been observed. These high translational energies occur for peripheral impacts, in which part of the projectile momentum is given to the nanoparticle as a whole. This so-called 'recoil' acceleration is quite a different mechanism than the one described here, which is based on acceleration by sputter emission. A comparison of these quite differing results demonstrates that besides the projectile impact energy, both projectile and target size are important parameters to determine the result of the collision.

3.4. 64 keV Impact

The 16 keV impacts considered above deliver their energy in the upper quarter of the nanoparticle. At higher projectile energies, the projectile penetrates deeper and delivers its energy closer to the nanoparticle centre. We studied the case of 64 keV projectiles. Here only central impacts were considered, since in more peripheral events, the projectiles generally will leave the nanoparticle before depositing all their energy inside it.

In four out of the nine impact events simulated, the projectile channelled through the nanoparticle depositing only little energy and causing only minor sputtering. In the remaining events, the average penetration depth was 9.0 ± 1.7 nm, i.e., the projectile energy was delivered in the nanoparticle centre. Note that if the entire projectile energy were used for nanoparticle heating, the final nanoparticle temperature amounted to 1003 K, i.e., below the melting temperature of Au. Fig. 6 displays cross-sectional views of the time evolution of the nanoparticle deformation and the sputtering process for a representative event with an average sputter yield ($Y = 3335$). It is seen that at this energy, the

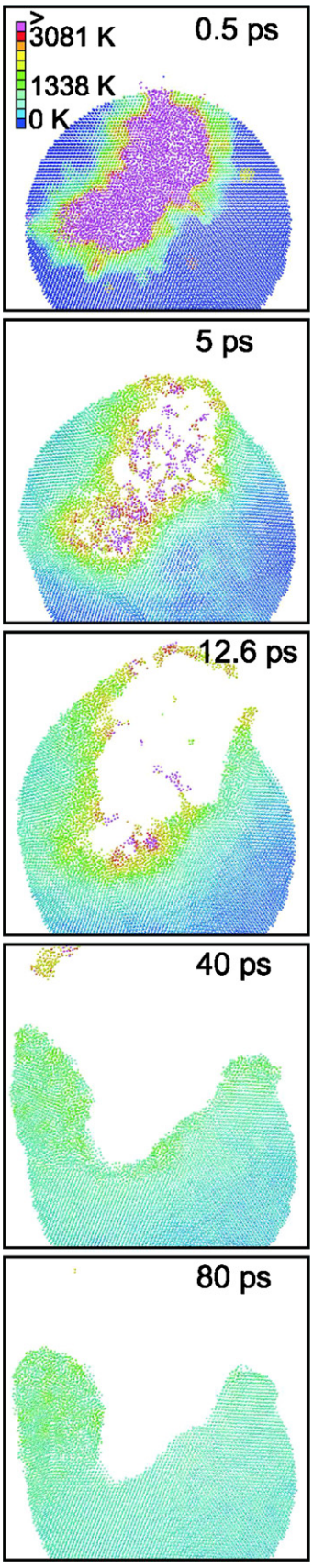

Fig. 6. Cross-sectional view of the time evolution of 64 keV Au central impact on the nanoparticle. A representative event has been selected with approximately average sputter yield. Colour denotes the local temperature.

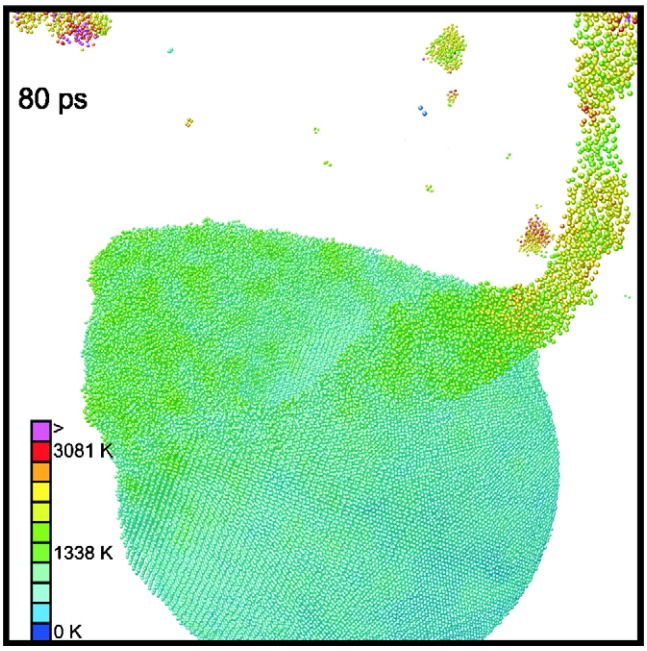

Fig. 7. Perspective view of the event of Fig. 6 at $t = 80$ ps after impact. Colour denotes the local temperature.

nanoparticle is almost destroyed. Fig. 7 gives a perspective view of the nanoparticle at a late time, 80 ps after impact.

Table 1 assembles quantitative information on the sputter yield. Besides the average sputter yield Y, we also show the standard deviation $\sigma = (\sum_i (Y_i - Y)^2/(n-1))^{1/2}$, where Y_i, $i = 1, \ldots, n$, denote the individual sputter yields. The standard deviation of the yield is astonishingly large. This is due to channelling events; roughly 50% of the trajectories penetrate the nanoparticle – or channel deep into the planar target – and leave only little energy for sputtering. Thus the sputter distribution is bimodal. *High-yield* events with an average yield of 5300 ± 2000 are opposed to *low-yield*, channelling events with $Y = 70 \pm 40$. The same feature shows up even more pronouncedly for impacts on the planar target with prolific sputter events with $Y = 1400 \pm 400$ clearly separated from channelling events with $Y = 9 \pm 1$.

4. Conclusions

Sputtering of nanoparticles shows interesting features when compared to the sputtering of a planar surface. We exemplify these features by considering the impact of 16 and 64 keV Au projectiles on a 20 nm Au nanoparticle.

(1) The sputter yield is more than doubled in comparison to the sputtering of a flat surface. The high yield is due to an energy deposition close to the nanoparticle surface. Sputtering is dominated by a strong spike contribution.
(2) The sputter yield depends only mildly on the impact parameter of the projectile. Even for ion impact at 9 nm distance from the centre, the sputter yield is reduced by only 20%.
(3) The momentum of the sputtered particles lets the remaining nanoparticle recoil in opposite direction with velocities of several m/s.

Acknowledgments

We are grateful to I. Baranov for discussions on the subject. We acknowledge the *Regionales Hochschulrechenzentrum Kaiserslautern* for making available their computing resources.

References

[1] W. Szymczak, N. Menzel, W.G. Kreyling, K. Wittmaack, Int. J. Mass Spectrom. 254 (2006) 70.
[2] U. Kirchner, R. Vogt, C. Natzeck, J. Goschnick, J. Aerosol Sci. 34 (2003) 1323.
[3] A. Bouchoule, Phys. World 6 (8) (1993) 47.
[4] E.M. Bringa, R.E. Johnson, Nucl. Instrum. Meth. B 193 (2002) 365.
[5] B.T. Draine, Annu. Rev. Astron. Astrophys. 41 (2003) 241.
[6] E.M. Bringa, R.E. Johnson, Astrophys. J. 603 (2004) 159.
[7] P. Sigmund, in: R. Behrisch (Ed.), Sputtering by Particle Bombardment I, Springer, Berlin, 1981, p. 9.
[8] R. Kissel, H.M. Urbassek, Nucl. Instrum. Meth. B 180 (2001) 293.
[9] I.A. Baranov, V.V. Obnorskii, S.O. Tsepelevich, Nucl. Instrum. Meth. B 35 (1988) 140.
[10] I. Baranov, S. Kirillov, A. Novikov, V. Obnorskii, M. Toulemonde, K. Wien, S. Yarmijchuk, V.A. Borodin, A.E. Volkov, Nucl. Instrum. Meth. B 230 (2005) 495.
[11] I. Baranov, S. Della-Negra, M. Fallavier, S. Kirillov, Y. LeBeyec, A. Novikov, V. Obnorskii, K. Wien, S. Yarmijchuk, Nucl. Instrum. Meth. B 245 (2006) 184.
[12] R. Kissel, H.M. Urbassek, Int. J. Mass Spectrom. 208 (2001) 29.
[13] S. Zimmermann, H.M. Urbassek, Nucl. Instrum. Meth. B 228 (2005) 75.
[14] S. Zimmermann, H.M. Urbassek, Nucl. Instrum. Meth. B 255 (2007) 208.
[15] T.J. Colla, H.M. Urbassek, Nucl. Instrum. Meth. B 164–165 (2000) 687.
[16] T.J. Colla, R. Aderjan, R. Kissel, H.M. Urbassek, Phys. Rev. B 62 (2000) 8487.
[17] E. Salonen, K. Nordlund, J. Keinonen, Nucl. Instrum. Meth. B 212 (2003) 286.
[18] J. Samela, K. Nordlund, Phys. Rev. B 76 (2007) 125434.
[19] J. Samela, K. Nordlund, Nucl. Instrum. Meth. B 263 (2007) 375.
[20] J. Samela, J. Kotakoski, K. Nordlund, J. Keinonen, Nucl. Instrum. Meth. B 239 (2005) 331.
[21] H. Gades, H.M. Urbassek, Phys. Rev. B 51 (1995) 14559.
[22] H.M. Urbassek, Nucl. Instrum. Meth. B 122 (1997) 427.
[23] H.M. Urbassek, in: P. Sigmund (Ed.), Ion Beam Science: Solved and Unsolved Problems, Royal Danish Academy of Sciences, Copenhagen, 2006, Mat. Fys. Medd. Dan. Vid. Selsk. 52, 433.
[24] H. M. Urbassek, in: R. Behrisch, W. Eckstein (Eds.), Sputtering by Particle Bombardment, Springer, Berlin, 2007, Top. Appl. Phys. 110, p. 189.
[25] J.F. Ziegler, J.P. Biersack, U. Littmark, The Stopping and Range of Ions in Solids, Pergamon, New York, 1985.
[26] I. Koponen, J. Appl. Phys. 72 (1992) 1194.
[27] R.S. Averback, M. Ghaly, Nucl. Instrum. Meth. B 90 (1994) 191.
[28] S. Zimmermann, Ph.D. thesis, University Kaiserslautern, 2006.
[29] W. Szymczak, K. Wittmaack, Nucl. Instrum. Meth. B 82 (1993) 220.
[30] C.P. Flynn, R.S. Averback, Phys. Rev. B 38 (1988) 7118.
[31] I. Koponen, Phys. Rev. B 47 (1993) 14011.
[32] I.A. Baranov, S. Della Negra, V.P. Domaratsky, A.V. Chemezov, A.C. Novikov, V.V. Obnorsky, M. Pautrat, C. Anders, H.M. Urbassek, K. Wien, S.V. Yarmiychuk, E.E. Zhurkin, Nucl. Instrum. Meth. B, submitted for publication.